Tropical Journal of Pharmaceutical Research March 2022; 21 (3): 485-494
ISSN: 1596-5996 (print); 1596-9827 (electronic)

Available online at http://www.tjpr.org
http://dx.doi.org/10.4314/tjpr.v21i3.5

Original Research Article

CK1α protects cardiomyocytes in sepsis-induced myocardial depression by repressing the interaction of ATG5 with myD88/NF-kappaB signaling

Hongpeng Sun, Yanmei Wu*
Department of Emergency, Guizhou Provincial People's Hospital, Guiyang 550000, Guizhou, China

For correspondence:* ***Email:* *wuyanmei8533@163.com,* ***Tel:*** *+86–17785131079*

Sent for review: 14 October 2021 *Revised accepted: 25 February 2022*

Abstract

Purpose: *To explore the effects of casein kinase 1α (CK1α) on cardiomyocytes in sepsis-induced myocardial depression.*
Methods: *Colorectal ligation puncture (CLP) surgery was performed for the establishment of the mouse model. Total RNAs of the lungs, kidneys, liver tissues and alveolar macrophages were extracted using TRIzol™ reagent, while gene expression analysis was performed by quantitative polymerase chain reaction (qPCR) following reverse transcription. Western blot was employed to evaluate protein expression, and echocardiography was conducted to assess cardiac function. Immunofluorescent assay was performed to determine the expression of p-FOXO3a in primary cardiomyocytes.*
Results: *Inhibition of CK1α impaired autophagy influx, and significantly increased inflammatory cytokines in H9C2 cells after lipopolysaccharide (LPS) treatment ($p < 0.05$). Moreover, aberrant activation of the Toll-like receptor 4(TLR4)/myD88/NF-kappaB pathway was observed in the H9C2 cell line after LPS treatment ($p < 0.05$). Immunoprecipitation analysis revealed an interaction between MyD88 and autophagy-related gene 5 (Atg5), and cardiac dysfunction in mice intravenously injected with an adenoviral vector containing shRNA (casein kinase 1 α) CSNK1A1 was suppressed ($p < 0.05$). In contrast, overexpression of CK1α remarkably improved cardiac systolic function ($p < 0.05$), the expression of inflammatory cytokines was repressed, and autophagy was enhanced in the hearts of mice with the specific overexpression of CSNK1A1 in cardiomyocytes ($p < 0.05$). In Atg5-deficient mice pretreated with DC661, the protective effect of adenoviral vector containing CK1α overexpression was eliminated.*
Conclusion: *CK1α protects cardiomyocytes during sepsis after the inhibition of TLR/MyD88/NF-kappaB pathway via interaction of Atg5 with MyD88. The results of the current study may provide new insights into the treatment of sepsis-induced myocardial depression.*

Keywords: *Casein kinase 1A1, Sepsis, Cadiomyocetes, Adenoviral vector, Echocardiography, Casein kinase 1α, Autophagy*

Tropical Journal of Pharmaceutical Research is indexed by Science Citation Index (SciSearch), Scopus, International Pharmaceutical Abstract, Chemical Abstracts, Embase, Index Copernicus, EBSCO, African Index Medicus, JournalSeek, Journal Citation Reports/Science Edition, Directory of Open Access Journals (DOAJ), African Journal Online, Bioline International, Open-J-Gate and Pharmacy Abstracts

INTRODUCTION

Myocardial depression induced by severe sepsis is a major complication in patients with sepsis, and is predicted to result in increased mortality [1,2]. Sepsis-induced myocardial dysfunction (SIMD) is characterized by increased left ventricular volume and reduced left ventricular

ejection fraction, as has been observed in > 40 % of patients with sepsis [3,4]. Although the appearance of SIMD is transient and reverses upon recovery from severe infection and sepsis, initial myocardial depression leads to severe cardiac shock, lessened response to fluid resuscitation, and increased CO despite initial treatment with cardiotonic drugs [4].

Despite previous studies, including those on the underlying etiology and pathophysiology, there is a limited understanding of SIMD that can be applied to improve clinical outcomes in septic patients with myocardial stunning. Moreover, there are several controversies regarding pathophysiological alteration, and the several potential therapeutic strategies based on the underlying biological mechanisms are inefficient [3,4]. Further research regarding the pathophysiology and biological mechanisms involved in sepsis-related myocardial depression is essential to identify novel and potential therapeutic targets.

Previous studies have demonstrated that the existence of some depressant substances could lead to myocardial stunning in septic animal models. Rat cardiomyocytes were treated with serum collected from patients with septic shock following the impairment of their contractile properties [5,6]. Several pro-inflammatory molecules (such as tumour necrosis factor (TNF)-α (TNF-α), cytokine interleukin-1 (IL-1β), and allergic toxin C5a) in patients with sepsis and septic shock act as mediators, and possess cardio-depressant properties *in vitro* [7,8]. These inflammatory mediators can aggravate oxidative stress in cardiomyocytes and promote oxidative modulation of certain vital proteins involved in the mechanical contractile of cardiomyocytes.

Myocardial dysfunction in children with meningococcal septic shock results in interleukin-6 (IL-6). Cardiomyocytes produces numerous molecules such as TNF-α, IL-1β, and nuclear protein high-mobility group box 1 (HMGB-1), many of which may be the cause of SIMD [9-11]. This production of inflammatory mediators by cardiomyocytes could be attributable to the local dysfunction of autophagy. Studies by Zhang J *et al* demonstrated that the administration of an AMP-activated protein kinase (AMPK) activator enhanced autophagy, thereby alleviating cardiotoxicity induced by LPS, and improving contractile properties and intracellular Ca^{2+} levels, revealing that the promotion of autophagy via AMPK can significantly attenuate impaired contractile properties and intracellular transportation of Ca^{2+} [12].

CK1α, a key negative mediator of the Wnt signaling pathway, and has been considered as a crucial inhibitory factor of tumors [13,14]. CK1α is a casein kinase 1 (CK1) protein that has extensive protein kinase activity, and is also a major component of Wnt/β-catenin signaling pathway. CK1α, a part of the β-catenin destruction complex, phosphorylates β-catenin at Ser45 for subsequent β-TrCP-mediated ubiquitination and proteasomal degradation. The ablation of CK1α with p53 deficiency may lead to increased tumorigenesis and an invasive phenotype in colorectal carcinoma [15]. Previous studies reported that CK1α may promote autophagy-related gene 7 (Atg7) transcription induced by forkhead transcription factor FOXO3a [16]. Blocking CK1α would then result in impaired Atg7-dependent autophagy, thereby initiating tumorigenesis in lung epithelial cells. Hence, the study regarded the Atg7-mediated autophagy pathway as an anti-tumorous mechanism dependent on FOXO3a-induced transcription of Atg7.

EXPERIMENTAL

Cell culture and animals

H9C2 cells (Fenghui Bio, Beijing, China) were purchased from Fenghui Biotech Ltd. and cultivated in low-glucose Dulbecco's Modified eagle medium (DMEM) with fetal bovine serum (FBS) (10 %) (Gibco, Rockville, MD, USA), penicillin (100 units/mL), and streptomycin (100 µg/mL) in 5 % CO_2 at 37 °C. Then, D4467, an inhibitor of CK1α, at a concentration of 10 µmol/L, was added to the cultured medium containing LPS (1 EU/mL), and then cultures were harvested for further experiments *in vitro*. C57/BL6 mice with a cardiac-specific deficiency of Atg5 ($Atg5^{-/-}$ mice) and wild type C57/BL6 mice were used in this study. All animal experiments were approved by the Medical Ethics Committee of Guizhou Provincial People's Hospital Animal Center (16GZ-no.032). All procedures were conducted in accordance with the 'Animal Research: Reporting in *In Vivo* Experiments guidelines 2.0.

RNA isolation and quantitative polymerase chain reaction (qPCR)

Total RNAs of lung, kidney, and liver tissues as well as the alveolar macrophages were extracted with the TRIzol™ reagent (Invitrogen, Carlsbad, CA, USA). Reverse transcription was performed using Reverse Transcription System. Gene expression analysis was performed using qPCR and following reverse transcription according to standard protocols. The sequences of primers

Table 1: The primers used for the quantitative PCR assays

Gene	Upstream primer	Downstream primer
IL-1b	GCAACTGTTCCTGAACTCAACT	ATCTTTTGGGGTCCGTCAACT
IL-6	GGCGGATCGGATGTTGTGAT	GGACCCCAGACAATCGGTTG
TNF-α	GCGCGATATGGTGTACCGCA	GTCAGTGGCATGGTGGTGAG
IL-8	GTGCACAGCCATCAAGCAAG	GACACGCCACACCCACCACC

used for mRNA expression analysis are shown in Table 1. The qPCR was performed on QuantStudio 5 with SYBR green PCR master mix. qPCR data were analyzed via the $2^{-\Delta\Delta Ct}$ method. The relative expression of the target genes was standardized to the expression of glyceraldheyde 3-phosphate dehydrogenase (GAPDH) mRNA and represented as fold change.

Echocardiography

Cardiac geometry and the functions of mice anesthetized using ~1 % of isoflurane were assessed with Phillips Sonos 5500 (Eindhoven, Netherlands). The cardiac tissue was imaged in the parasternal long-axis view. The M mode cursor was perpendicular to the posterior wall of the left ventricle (LV) at papillary muscle level and interventricular septum. LV anterior and posterior wall dimensions during diastole (LVPWd) were recorded in conformity with the method provided by the American Society of Echocardiography (ASE). Fractional shortening (FS) was calculated as in Eq 1.

$$FS = \frac{(LVEDD - LVESD)}{LVEDD} \quad \ldots\ldots\ldots (1)$$

where LVEDD and LVESD are the LV end-diastolic and end-systolic diameters, respectively.

Transiency of intracellular Ca^{2+}

Free Ca^{2+} in cardiomyocytes were combined with Fura-2/AM (0.5 μmol/L), and fluorescence was measured via a photo multiplier tube. Cardiomyocytes were imaged via a Fluor 40× oil objective. Cells were exposed to light and went through a filter (360 or 380 nm), while induced to contract at 0.5 Hz. Fluorescence (480 - 520 nm) emissions were monitored after cells were illuminated at 360 nm for 0.5 sec and then at 380 nm for 3 milliseconds (ms) at a frequency of 333 Hz. The 360 nm excitation scan was conducted twice, and qualitative variation of intracellular Ca^{2+} levels was reflected by the value of Fura-2 fluorescence intensity at 360 nm divided by the value at 380 nm. The decay rate (DR) of fluorescence, an index of the clearance level of Ca^{2+}, was calculated via a single exponential curve fitting.

Protein extraction and Western blot

Proteins from cultivated H9C2 cells were prepared in radioimmunoprecipitation assay (RIPA) lysis buffer (Beyotime, Shanghai, China) according to standard protocols. An equal amounts of protein (30 ug) were separated with sodium dodecyl sulphate-polyacrylamide gel electrophoresis (SDS-PAGE), and then transferred to polyvinylidene fluoride (PVDF) membranes (Millipore, Billerica, MA, USA), which were blocked with 5 % milk in TBST at 37 °C for 2 h and incubated with the following primary antibodies at 4 °C overnight: anti-LC3-I/II (1:500, Cat: 4599, CST, Danvers, MA, USA); anti-AMPK (1:1000, Cat: ab3759, Abcam, Cambridge, MA, USA); anti-p-AMPK (1:1000, Cat: NB100-92711, Novus Biologicals, Littleton, CO, USA); anti-Atg5 (1:1000, Cat: NB110-53818, Novus Biologicals, Littleton, CO, USA); anti-Atg7 (1:1000, Cat: MAB6608, R&D Systems, Minneapolis, MN, USA); anti-Beclin (1:1000, Cat: GTX37770, GeneTex, Shanghai, China); anti-mTORC1 (1:2000, Cat: ab25880, Abcam, Cambridge, MA, USA); anti-p-mTORC1 (1:1000,Cat: 2972, CST, Danvers, MA, USA); anti-MyD88 (1:1000,Cat: NB100-56698, Novus Biologicals, Littleton, CO, USA); anti-FOXO3a (1:3000, Cat:10849-1-AP, Proteintech, Rosemont, IL, USA); anti-p-FOXO3a (1:1000, Cat: 9465, CST, Danvers, MA, USA); anti-NF-κB (1:1500, Cat: 14220-1-AP, Proteintech, Rosemont, IL, USA); anti-p-NF-κB (1:500, Cat: sc-33022, Santa Cruz Biotechnology, Santa Cruz, CA, USA); anti-IκBκ (1:1000, Cat: sc-33022, Santa Cruz Biotechnology, Santa Cruz, CA, USA); anti-GAPDH (1:1000, sc-47778 Santa Cruz Biotechnology, Santa Cruz, CA, USA); anti-caspase-8 (1:1,000, Cat: 9504, CST, Danvers, MA, USA); and anti-caspase-3 (1:1,000, CAT: ab32499, Abcam, Cambridge, MA, USA). After they were washed several times, the membranes were incubated with secondary antibody at 25 °C for 60 min. Chemiluminescence was used to visualize blotted bands, and the gray values of the protein bands were measured using the ECL Fuazon Fx (Vilber Lourmat, Paris, France).

Colorectal ligation puncture (CLP) surgery

The CLP surgery was performed as previously described [17]. Mice were anesthetized with 50

mg/kg ketamine (Tocris Biosecience, Bristol, England) in combination with xylazine (Rompun®) (10 mg/kg), and the cecum was 100 % ligated with sterile 10 mm stainless steel surgical clips outside the abdominal cavity. The puncture was performed three times with a 22-gauge needle. The intestinal tube was repositioned outside the abdominal cavity, which was closed with a 4-0 sterile suture. The abdominal cavity was opened only in the sham mice, but without ligation and puncture at the site of the cecum.

Immunofluorescent assay

For immunostaining, cardiomyocytes were fixed with 4 % paraformaldehyde and then permeabilized with 0.01 % Triton X-100 at RT. Both processes lasted for 10 min. Subsequently, the resultant cells were incubated with 5 % BSA at 25 °C for 0.5 h, treated with anti-p-FOXO3a (1:1500), and then used to determine the expression of p-FOXO3a in primary cardiomyocytes after induction with LPS. Furthermore, the cells were incubated at 37 °C for another hour with anti-rabbit IgG (H+L) labelled with fluorescein isothiocyanate (FITC). Finally, the cells were viewed under a laser scanning microscope.

Oxidation of SERCA2a

Cardiac tissues were treated with ultrasound (Use ice bath, 400 w, break 5 s and stop 5 s, 5 times) and then dissolved in the CHAPSbuffer (Cat: HZ25-01380, Shanghai Huzhen Industrial Co., Ltd., Shanghai, China) supplemented with CHAPS (0.5 %), Tris-HCl (10 mmol/L), DTT (50 mmol/L), and saccharose (0.3 mol/L). After centrifugation, the tissues were incubated with anti-SERCA2a (1:1000, Cat: 13985-1-AP, Proteintech, Rosemont, IL, USA) overnight. A slurry of IgG agarose was added, and the mixture was stirred for 2 h. All the processes mentioned above were performed at a low temperature (4 °C). Oxidative SERCA2a reacts with dinitrophenylhydrazine, and its byproduct was detected with an anti-DNP antibody (1:1000, Cat: D9781, Sigma-Aldrich, St. Louis, MO, USA). Total expression of SERCA2a after immunoprecipitation was used to standardize protein load.

Transfection of adeno-associated virus vectors

The construction of an adeno-associated virus serotype 9 (AAV9) vector, characterized by partial cardiac specificity, encoding CSNK1A1 and green fluorescent protein was performed using the Shanghai Jikai Gene Chemical Technology Co., Ltd. (Shanghai, China). The AAV9 vector was used for the overexpression of CSNK1A1 in H9C2 cells and in the hearts of septic rats via intravenous injection in the jugular vein. In addition, AAV9 vectors containing siRNA-CSNK1A1 were added via intravenous injection in the jugular vein prior to the operation on CLP mice. The negative control was constructed using a scrambled sequence not capable of encoding the target protein. Transfection was performed as previously described [18]. H9C2 cells were inoculated on 24-well plates (~5000 cells/well), incubated at 37 °C for 24 h, and then transfected with AAV9 vectors for 10 to 12 h as per the manufacturer's instructions. Cells with green fluorescence indicated stable transduction with the AAV9 vector. In total, > 85 % of cells were positive for green fluorescence as visualized by fluorescence microscopy at 48 h, thereby indicating the successful establishment of cell line models, classified as the negative control and AAV9-CSNK1A1 (overexpression). The green fluorescent signals indicated the establishment of CSNK1A1 overexpression in the heart tissues of septic rats as well.

Determination of shortening and re-lengthening of cells

Mechanical performances of cardiomyocytes were evaluated as previously elucidated [19], and were placed in a chamber equipped on platforms of an inverted microscope and incubated at 25 °C with a buffer (pH 7.4) containing HEPES, glucose, $MgCl_2$, $CaCl_2$ NaCl, and KCl. The cells were treated with a suprathreshold voltage (0.5 Hz) for 3 ms, which triggered muscle contractions. Myocytes were observed using an IonOptix MyoCam camera. The corresponding software was applied to monitor the variation of cell length during shortening and re-lengthening phases. The shortening and re-lengthening of cells was evaluated with the following indexes: peak shortening (PS), maximum speed of shortening and re-lengthening (± dL/dt), time-to-PS (TPS), and time-to-90 % re-lengthening (TR90).

Statistical analysis

All experiments were conducted in parallel no less than 5 times, and the data obtained in the study are presented as mean ± (standard deviation SD). Unpaired *t*-tests were conducted to determine statistical differences between the two groups. Analysis of variance (ANOVA) was applied to compare the data of the two groups from multiple aspects. $P < 0.05$ indicated

statistical significance. The log-rank test was used on the survival curves (Kaplan-Meier) in the study. Statistical analysis was conducted via the Statistical Product and Service Solutions (SPSS) 17.0 software (SPSS Inc, Chicago, IL, USA).

RESULTS

Inhibition of CK1α did not affect the classical autophagy pathway but down-regulated autophagy influx in cardiomyocytes

A pharmacological inhibitor (D4467) was first administered (D4467) in the H9C2 cell line (human cardiomyocytes cells) to repress CK1α, then the phosphorylation levels of proteins related to autophagy—p-AMPK and p-mTORC1 in pretreated cardiomyocytes treated with CK1α inhibitor were examined. The results showed that the inhibition of CK1α did not affect the expression of proteins involved in the autophagy pathway (Figure 1 A and B). There was no difference in the phosphorylation levels of p-mTORC1 and p-AMPK between cardiomyocytes suppressed for CK1α or not (Figure 1 C). The data demonstrated that CK1α might not affect the upstream activation of classical autophagy-related pathways. Intriguingly, the expression of autophagy markers such as Atg5, Atg7, and Beclin-1, were significantly decreased when compared with controls (Figure 1 D). The nuclear translocation and phosphorylation of FOXO3a was significantly decreased in cardiomyocytes with inhibited CK1α (Figure 1 E and F). The autophagy influx was inhibited in cardiomyocytes treated with CK1α-siRNA and D4467 as manifested on an increased ratio of LC3-I/II (Figure 1 G). These data revealed that deficiency of CK1α could lead to the inhibition of FOXO3a-dependent autophagic activation and expression of autophagy-related proteins.

Inhibition of CK1α aggravated the activation of TLR4/MyD88/NF-κB inflammatory pathway in cardiomyocytes

The activation of autophagy of cardiomyocytes with inhibited CK1α was significantly repressed. To examine whether the phenomenon existed in cardiomyocytes, coimmunoprecipitation assays were performed in H9C2 cells deficient of Atg5 (siAtg5), and then treated with LPS. Similar results were observed in HEK 293T cells (Figure 2 A). In cells administered with D4467, Atg5 interacted with MyD88 because of the coimmunoprecipitation with MyD88 in the cells treated with D4467 (Figure 2 B), which demonstrated that Atg5 interacted with MyD88 in cardiomyocytes and then inhibited the MyD88/NF-κB signaling pathway. Results

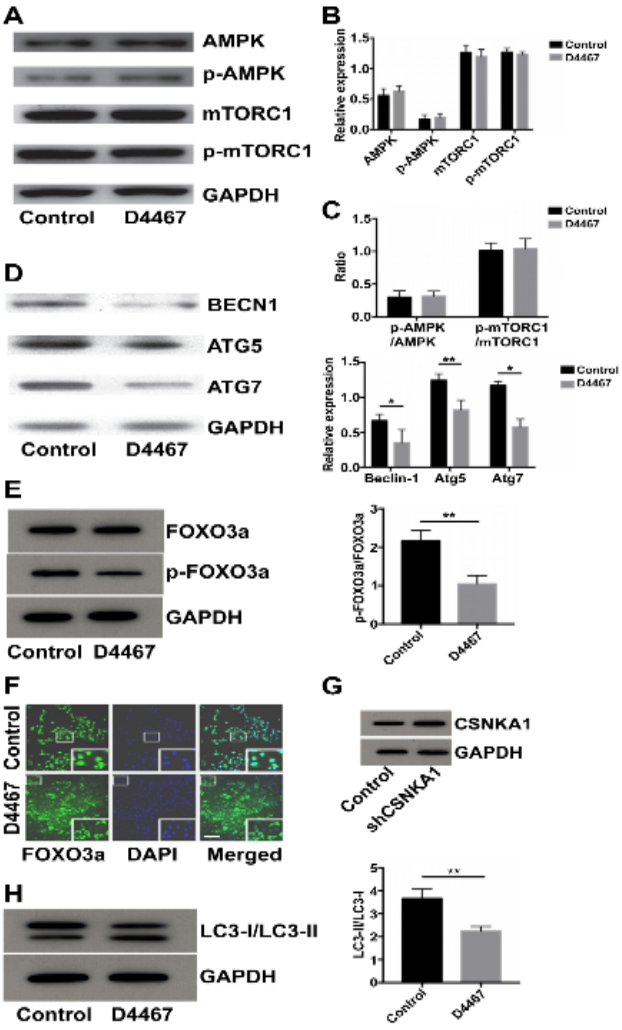

Figure 1: Inhibition of CK1α did not affect classical autophagy, but down-regulated autophagy influx in cardiomyocytes. (A) The expression of proteins involved in the classical autophagy signaling pathway in the LPS-induced H9C2 cell line. (B) The expression of mTORC1, p-mTORC1, AMPK, and p-AMPK in LPS-induced H9C2 cells. (C) Altered phosphorylation levels of p-AMPK and p-mTORC1 in LPS-induced H9C2 cells. (D) Autophagy-related proteins in LPS-induced H9C2 cells after administration of the CK1α inhibitor D4467. (E) FOXO3a and phosphorylated FOXO3a in LPS-induced H9C2 cells after administration of the CK1α inhibitor D4467. (F) Decreased co-localization of FOXO3a with nuclei in cells treated with the CK1α inhibitor D4467 was observed. (G) Representative figures of the overexpression of CSNK1A1 in tissue. (H) immunoblot assays of LC3-I/IIn H9C2 cells. All experiments were repeated at least five times

showed that the expression of p-NF-κB and IκBκ were significantly aggravated in H9C2 cells treated with D4467 (Figure 2 C). The expression of inflammatory cytokines was then measured by qPCR, and significantly increased expression was found in D4467-treated cardiomyocytes

(Figure 2 D). The concentrations of cytokines in the supernatant were also significantly increased (Figure 2 E). These data illustrated that CK1α inhibition led to the activation of the MyD88/NF-κB signaling pathway and excessive cytokine production.

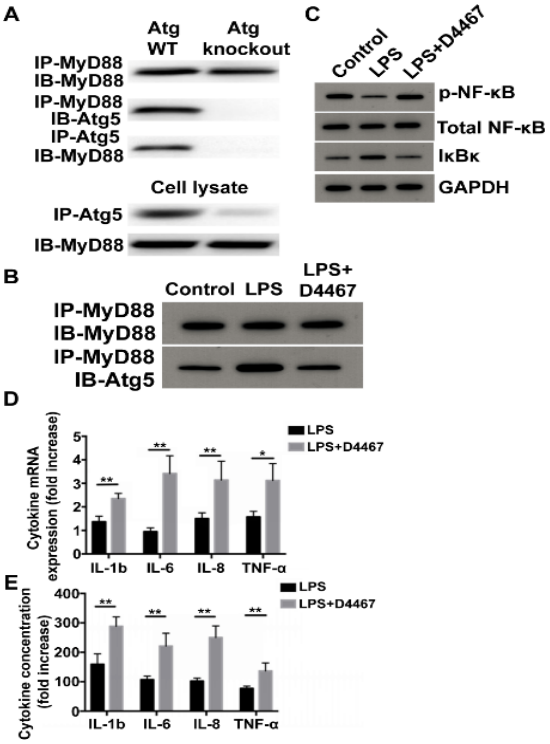

Figure 2: Inhibition of CK1α aggravated the activation of TLR4/MyD88/NF-κB inflammatory pathway in cardiomyocytes. (A) Co-IP assay of MyD88 and NF-κB in H9C2 cells deficient for Atg5 and treated with LPS. (B) The Co-IP assay of MyD88 and NF-κB in LPS-treated H9C2 cells with CK1α inhibitor, D4467. (C) Phosphorylation and expression levels of proteins associated with the NF-κB signaling pathway. (D) Levels of expressions of inflammatory cytokines secreted by cardiomyocytes in LPS-treated H9C2 cells. (E) Concentrations of cytokines in supernatants was also significantly increased in cardiomyocytes treated with D4467. All experiments were repeated at least five times

CK1α inhibition worsens cardiac contractile mechanical properties

To further investigate whether the inhibition of CK1α could lead to changes in contractile properties and intracellular Ca^{2+} transportation, cellular shortening and intracellular Ca^{2+} transiency were detected in the LPS-induced H9C2 cells overexpressing CSNK1A1. LPS suppressed the contractile function of cardiomyocytes, which was reflected in reduced PS and maximum speed of shortening/re-lengthening, as well as prolonged TR90 in the H9C2 cells (Figure 3 A – D).

However, CK1α improved the contractile abnormality of cardiomyocytes induced by LPS to a certain extent, without causing changes in resting cell length (RCL) and TPS (Figure 3 E–F). To study the underlying mechanism and illustrate the improving effect of CK1α against cardiac dysfunction caused by LPS exposure, intracellular Ca^{2+} transiency was measured. Once electrically stimulated, the release of Ca^{2+} in cardiomyocytes decreased. After LPS treatment, cardiomyocytes prolonged the decay time of intracellular Ca^{2+}, while simultaneously not changing resting intracellular Ca^{2+} (resting FFI). CK1α hardly reduced the effect caused by LPS on the properties of intracellular Ca^{2+} (Figure 4 A – C). The oxidative intracellular Ca^{2+} protein SERCA2a was also significantly increased, but the total protein expression was similar in H9C2 cells with or without the overexpression of CK1α (Figure 4 D), which demonstrated that the oxidation of SERCA2a may be involved in contractile stunning after LPS treatment and CK1α could through inhibition of inflammatory and oxidative stress.

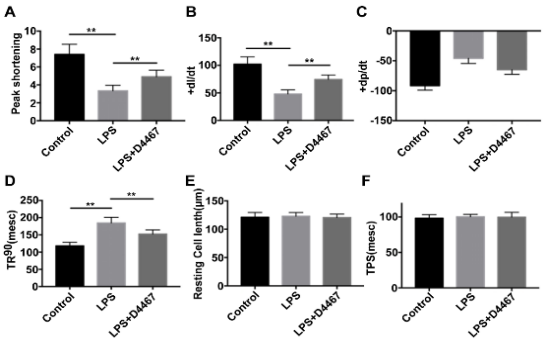

Figure 3: CK1α inhibition worsened cardiac contractile mechanical properties. The contractile properties of LPS-induced cardiomyocytes treated with/without D4467. (A) PS; (B) maximum speed of shortening (+ dL/dt); (C) maximum speed of re-lengthening (− dL/dt); (D) TR90; (E) RCL; and (F) TPS. All experiments were repeated at least five times

Cardiac-specific overexpression of CK1α improved cardiac function in septic mice

In the sepsis mice model, chocardiography test was performed to evaluate cardiac function after administering an AAV9 vector that either overexpresses or suppresses CSNK1A1. Echocardiographic evaluation revealed that cardiac overexpression of CK1α significantly improved left ventricular dilation and decreased FS (Figure 5 A and B) without changes in LV posterior wall thickness in diastole (LVPWd) and

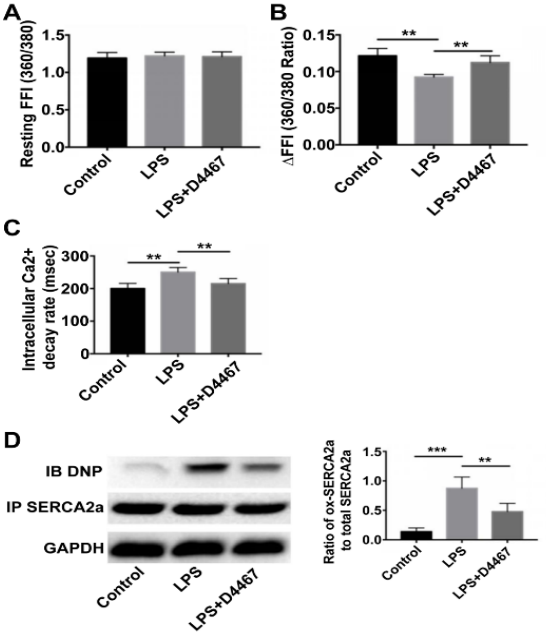

Figure 4: Properties of intracellular Ca^{2+}, superoxide production in LPS-induced cardiomyocytes, and SERCA oxidation. (A) FFI; (B) change in FFI (ΔFFI); (C) DR; (D) oxidative and total levels of SERCA2a. Left panel: typical gel blot levels of SERCA2a and DNP; right panel: the semi-quantitative analysis of the ratio of oxidative-SERCA2a to SERCA2a. All experiments were repeated at least five times

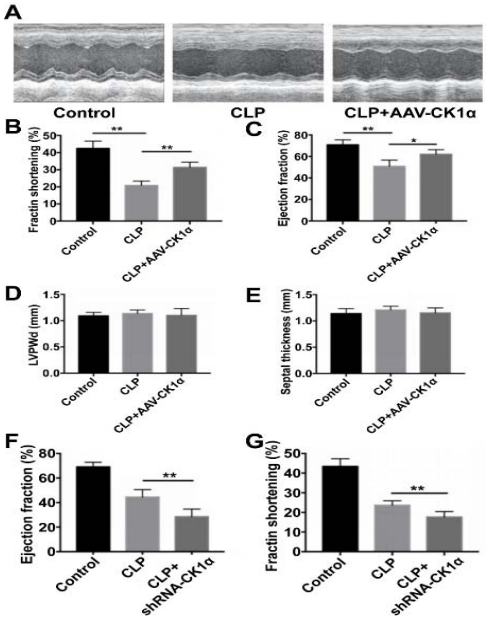

Figure 5: The echocardiographic changes after overexpression or knockout of CK1α in mice with sepsis-induced myocardial depression. (A) Representative echocardiography of the control, CLP, and CLP mice with myocardial specific overexpression of CK1α (shRNA-CK1α); (B) FS; (C) LVEF; (D) LVPWd; (E) septal thickness; (F and G) the alteration of echocardiographic parameters in CLP mice with or without myocardial specific transfection of siRNA-CK1α. There were significantly decreased LVEF (F) and FS (G) in CLP mice transfected with myocardial specific siRNA-CK1α was observed

septal thickness (Figures 5 C-E). Cardiac-specific transfection of siRNA-CSNK1A1 deteriorated left ventricular dilation and decreased FS (Figure 5 F and G). The data demonstrated the potential therapeutic value of CK1α in the sepsis-induced myocardial stunning and dysfunction.

CK1α did not improve cardiac function in septic mice with Atg5 deficiency

To further study the role of autophagy marker Atg5 in myocardial stunning during sepsis, mice were treated with an AAV9 vector to cause cardiac-specific overexpression of CK1α. It was discovered that mice with Atg5 deficiency had worse cardiac function and higher mortality in the follow-up period than WT mice (Figures 6A and 6B), and AAV9-CSNK1A1 did not improve cardiac functions (Figure 6C). These data demonstrated that Atg5 is indispensable due to its protective effect from the overexpression of CK1α in cardiomyocytes from myocardial stunning and systolic dysfunction.

DISCUSSION

Autophagy plays a crucial part in maintaining organismal homeostasis, and is an evolutionarily conserved catabolic process [20]. Autophagy regulates cellular protein and organelle turnover through lysosome-dependent degradation, and supplies cells with macromolecular precursors and energy. Abnormal autophagy results in homeostasis disorders and various diseases such as malignant tumor, inflammatory diseases and cardiovascular diseases [20]. In addition, the dysregulation of autophagy may promote uncontrolled inflammatory responses, such as myocardial inflammation after myocardial infarction. According to previous studies, insufficient activation of autophagy is associated with the impairment of contractile properties in cardiomyocytes [12,19]. In this study, it was discovered that CK1α attenuates inflammatory cytokine production in cardiomyocytes, alleviates the impairment of the contractile properties of cardiomyocytes, and improves myocardial depression via the promotion of autophagy in LPS-induced cardiomyocytes and septic mice. The mechanism involved in the activation is independent of the alteration of the classical signaling pathway related to autophagy regulation: it might be due to the FOXO3a-dependent transcription of autophagy-related

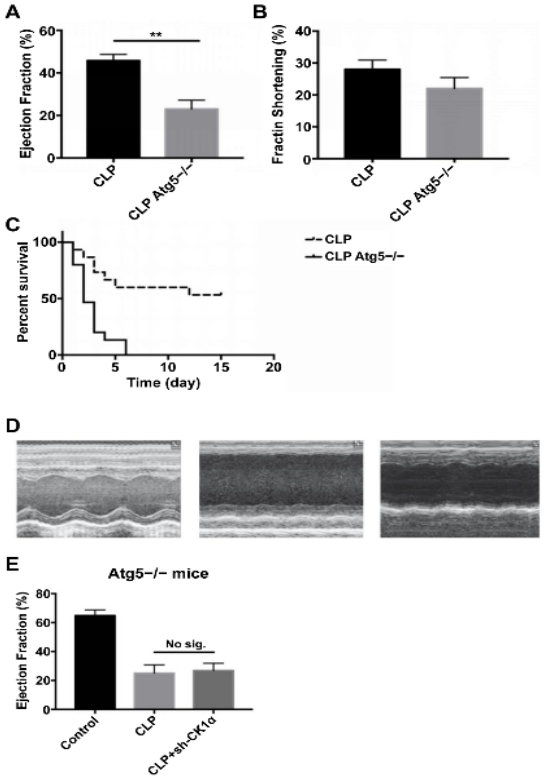

Figure 6: Echocardiographic changes and survival analysis after overexpression or knockout of CK1α in Atg5 −/− mice with sepsis-induced myocardial depression (A-B). The echocardiographic changes, i.e. LVEF (A) and FS (B), in WT and Atg5 $^{-/-}$ mice with sepsis-induced myocardial depression. (C) Survival curve in the follow-up period (15 days after CLP) in WT and Atg5 −/− mice with sepsis-induced myocardial depression. (D) Representative echocardiographic images and quantitative analysis from all three groups in Atg5 $^{-/-}$ mice with sepsis-induced myocardial depression: controls, CLP mice, and CLP mice with myocardial specific overexpression of CK1α. (E) myocardial specific overexpression of CK1α(Sh-CK1α) did not significantly improve LVEF and FS in ATG5 −/− mice after CLP

proteins

In general, adverse conditions such as infection and nutrient deficiency could result in autophagy [20]. The activation of autophagy due to these stresses plays a protective role and maintains physiological homeostasis [20]. Vesicle nucleation is induced by an activated ULK1 complex, which is released due to mTOR inhibition. The PI3K/Akt-mTOR signaling pathway, an important negative regulator for the formation of autophagosomes, is closely correlated with mTOR activity.

Activated TSC2 suppresses the formation of the TSC1/TSC2 heterodimer and then activates TORC1 [21]. Once activated, mTOR induces protein synthesis by phosphorylating P70S6K and 4EBP-1, two crucial translation regulators, so as to modulate autophagy, cell proliferation and growth. AMPK, which has been found to be involved in cardiovascular diseases and cellular stress, is another crucial signaling pathway in the promotion of autophagy. Currently, many studies have demonstrated that the activation of AMPK may cause autophagy via the downregulation of mTOR. Activated AMPK suppresses TORC1 by phosphorylating and activating TSC2 as well as inducing autophagy by directly phosphorylating ULK1 [22]. In the current study, the human gastric cancer cell responses in the process of VES-induced autophagy was explored, in addition to whether the process was associated with the accumulation of AMPK. In addition, the existence of a possible interaction between Akt/mTOR and AMPK signaling pathways was also explored. The study may entrench an understanding of the role played by autophagy in the antitumor activity mediated by VES. Therefore, expression and phosphorylation mTORC1 and AMPK could reflect in the activation of the classical autophagy signaling pathway. Unexpectedly, no alteration of activation or inhibition in these pathways was observed, which suggested that CK1α could not directly aggravate autophagy that is dependent on the mTORC1 and AMPK signaling pathway.

Autophagy-relevant genes such as LC3B, GABARAPs and Atg4B may be directly modulated by FOXO3A, which can be phosphorylated at Ser321 and Ser318. Previous studies have revealed that D4476 or siRNA treatment suppressed CK1α to upregulate the DEP domain-containing mTOR-interacting protein (DEPTOR), suppress mTOR signaling, and induced autophagy. CK1α is a crucial regulator of autophagy flux, and effector nuclease-mediated CSNK1A1 knockout promoted the turnover of protein. Previous studies also demonstrated that CSNK1A1 knockdown induced autophagy flux [23]. Therefore, CK1α exhibited downregulation effects on autophagy.

However, there existed differences in the action modes of CK1α between non-small lung cancer (NSCLC) and colon cancer caused by RAS. Overexpression of CK1α effectively induced autophagy flux in NSCLC, and stabilizes PTEN and phosphatase by discontinuing PTEN phosphorylation, antagonizing neural precursor cells, as well as downregulating NEDD4-1-induced PTEN polyubiquitination, which inhibits the growth of NSCLC cells. These show that CK1α has dual functions in regulating autophagy. In this study, it was discovered that CK1α

promotes autophagy in cardiomyocytes treated with LPS by promoting nuclear translocation, phosphorylating FOXO3a, and increasing the expression of autophagy-relevant proteins. This discrimination may be attributed to the distinct influence of CK1α on the mTORC1 signaling pathway and phosphorylation levels of FOXO3a. In cardiomyocytes, CK1α might not lead to upregulation of DEPTOR and affect the activation of mTORC1 signaling. Conversely, CK1α promotes the PTEN/AKT/FOXO3A/Atg7 axis and induces increased autophagic influx as observed in NSCLC cells previously reported.
Previous studies indicated that the loss of Atg5 promoted the formation of MyD88 condensed structure, and the occurrence of some MyD88-mediated signaling events [24]. Atg5 may interact with, but not degrade MyD88. Therefore, when stimulated with LPS, the signaling relevant for MyD88 may be activated, and may then induce the formation and conversion of LC3, suggesting that Atg5 exerted a regulatory effect on signaling relevant to MyD88, perhaps by interacting with MyD88, and subsequently directly blocking MyD88/NF-κB signaling, but not via autophagic processes. Although the increased autophagy process is dependent on the nuclear translocation of FOXO3a, CK1α attenuated inflammation and oxidization of SERCA2a.

CONCLUSION

The findings of this study offer some insight into the regulation of autophagy and inflammation in sepsis-induced myocardial depression. These results show that CK1α decreases myocardial inflammation and improves myocardial depression which are dependent on the activation of autophagy and the blocking of MyD88/NF-κB signaling. Thus, this study reveals the direct association between classical inflammatory signaling and autophagy processes, and hence provides a novel potential therapeutic strategy for SIMD.

DECLARATIONS

Acknowledgement

This work was supported by Science and Technology Bureau of Dalian (no. 2015E12SF161).

Competing interests

There is no conflict of interest to disclose with regard to this work.

Contribution of authors

We declare that this work was done by the authors named in this article and all liabilities pertaining to claims relating to the content of this article will be borne by the authors. Hongpeng Sun and Yanmei Wu contributed equally to this work.

REFERENCES

1. *Antonucci E, Fiaccadori E, Donadello K, Taccone FS, Franchi F, Scolletta S. Myocardial depression in sepsis: from pathogenesis to clinical manifestations and treatment. J Crit Care 2014; 29(4): 500-511.*
2. *Kakihana Y, Ito T, Nakahara M, Yamaguchi K, Yasuda T. Sepsis-induced myocardial dysfunction: pathophysiology and management. J Intensive Care 2016; 4: 22.*
3. *Liu YC, Yu MM, Shou ST, Chai YF. Sepsis-Induced Cardiomyopathy: Mechanisms and Treatments. Front Immunol 2017; 8: 1021.*
4. *Tsolaki V, Makris D, Mantzarlis K, Zakynthinos E. Sepsis-Induced Cardiomyopathy: Oxidative Implications in the Initiation and Resolution of the Damage. Oxid Med Cell Longev 2017; 2017: 7393525.*
5. *Romero-Bermejo FJ, Ruiz-Bailen M, Gil-Cebrian J, Huertos-Ranchal MJ. Sepsis-induced cardiomyopathy. Curr Cardiol Rev 2011; 7(3): 163-183.*
6. *Essandoh K, Yang L, Wang X, Huang W, Qin D, Hao J, Wang Y, Zingarelli B, Peng T, Fan GC. Blockade of exosome generation with GW4869 dampens the sepsis-induced inflammation and cardiac dysfunction. Biochim Biophys Acta 2015; 1852(11): 2362-2371.*
7. *Nejati A, Doustkami H, Babapour B, Ebrahimoghlou V, Aslani MR. Serum Correlation of Nesfatin-1 with Angiographic, Echocardiographic, and Biochemical Findings in Patients with Coronary Artery Disease. Iran Red Crescent Me 2021; 23(3): e245.*
8. *Ndongson-Dongmo B, Heller R, Hoyer D, Brodhun M, Bauer M, Winning J, Hirsch E, Wetzker R, Schlattmann P, Bauer R. Phosphoinositide 3-kinase gamma controls inflammation-induced myocardial depression via sequential cAMP and iNOS signalling. Cardiovasc Res 2015; 108(2): 243-253.*

9. Ferdous A, Battiprolu PK, Ni YG, Rothermel BA, Hill JA. FoxO, autophagy, and cardiac remodeling. J Cardiovasc Transl Res 2010; 3(4): 355-364.
10. Chien WS, Chen YH, Chiang PC, Hsiao HW, Chuang SM, Lue SI, Hsu C. Suppression of autophagy in rat liver at late stage of polymicrobial sepsis. Shock 2011; 35(5): 506-511.
11. Makwana N, Baines PB. Myocardial dysfunction in meningococcal septic shock. Curr Opin Crit Care 2005; 11(5): 418-423.
12. Zhang J, Zhao P, Quan N, Wang L, Chen X, Cates C, Rousselle T, Li J. The endotoxemia cardiac dysfunction is attenuated by AMPK/mTOR signaling pathway regulating autophagy. Biochem Biophys Res Commun 2017; 492(3): 520-527.
13. Jiang J. CK1 in Developmental Signaling: Hedgehog and Wnt. Curr Top Dev Biol 2017; 123: 303-329.
14. Li B, Orton D, Neitzel LR, Astudillo L, Shen C, Long J, Chen X, Kirkbride KC, Doundoulakis T, Guerra ML, et al. Differential abundance of CK1alpha provides selectivity for pharmacological CK1alpha activators to target WNT-dependent tumors. Sci Signal 2017; 10(485).
15. Chang CH, Kuo CJ, Ito T, Su YY, Jiang ST, Chiu MH, Lin YH, Nist A, Mernberger M, Stiewe T, et al. CK1alpha ablation in keratinocytes induces p53-dependent, sunburn-protective skin hyperpigmentation. Proc Natl Acad Sci U S A 2017; 114(38): E8035-E8044.
16. Yi L, Yang F, Yi Z. Delicaflavone induces apoptosis and autophagy, and improves the cytotoxicity of multiple myeloma cells to cisplatin by inactivating the AKT/mTOR pathway. Trop J Pharm Res 2021; 20(5): 967-972.
17. Cotroneo TM, Hugunin KM, Shuster KA, Hwang HJ, Kakaraparthi BN, Nemzek-Hamlin JA. Effects of buprenorphine on a cecal ligation and puncture model in C57BL/6 mice. J Am Assoc Lab Anim Sci 2012; 51(3): 357-365.
18. Schuster DJ, Dykstra JA, Riedl MS, Kitto KF, Belur LR, McIvor RS, Elde RP, Fairbanks CA, Vulchanova L. Biodistribution of adeno-associated virus serotype 9 (AAV9) vector after intrathecal and intravenous delivery in mouse. Front Neuroanat 2014; 8: 42.
19. Zhao X, Qi H, Zhou J, Xu S, Gao Y. P27 Protects Cardiomyocytes from Sepsis via Activation of Autophagy and Inhibition of Apoptosis. Med Sci Monit 2018; 24: 8565-8576.
20. Jain M, Iqbal H, Yadav P, Singh H, Chanda D, Jagavelu K, Hanif K. Autophagy inhibition by chloroquine prevents increase in blood pressure and preserves endothelial functions. Trop J Pharm Res 2020; 19(4): 789-796.
21. Liu M, Zeng T, Zhang X, Liu C, Wu Z, Yao L, Xie C, Xia H, Lin Q, Xie L, et al. ATR/Chk1 signaling induces autophagy through sumoylated RhoB-mediated lysosomal translocation of TSC2 after DNA damage. Nat Commun 2018; 9(1): 4139.
22. Agarwal S, Bell CM, Rothbart SB, Moran RG. AMP-activated Protein Kinase (AMPK) Control of mTORC1 Is p53- and TSC2-independent in Pemetrexed-treated Carcinoma Cells. J Biol Chem 2015; 290(46): 27473-27486.
23. Amaravadi RK. Transcriptional regulation of autophagy in RAS-driven cancers. J Clin Invest 2015; 125(4): 1393-1395.
24. Into T, Horie T, Inomata M, Gohda J, Inoue JI, Murakami Y, Niida S. Basal autophagy prevents autoactivation or enhancement of inflammatory signals by targeting monomeric MyD88. Sci Rep 2017; 7(1): 1009.